Dyes and Pigments 91 (2011) 237–247

Contents lists available at ScienceDirect

Dyes and Pigments

journal homepage: www.elsevier.com/locate/dyepig

Three new five-coordinated mercury (II) dyes: Structure and enhanced two-photon absorption

Hongping Zhou [a,*], Feixia Zhou [a], Peng Wu [a], Zheng Zheng [a], Zhipeng Yu [a], Yixin Chen [a], Yulong Tu [a], Lin Kong [a], Jieying Wu [a], Yupeng Tian [a,b,c]

[a] Department of Chemistry, Anhui University and Key Laboratory of Functional Inorganic Materials Chemistry of Anhui Province, 230039 Hefei, PR China
[b] State Key Laboratory of Crystal Materials, Shandong University, 250100 Jinan, PR China
[c] State Key Laboratory of Coordination Chemistry, Nanjing University, 210093 Nanjing, PR China

ARTICLE INFO

Article history:
Received 6 November 2010
Received in revised form
17 March 2011
Accepted 17 March 2011
Available online 23 March 2011

Keywords:
Single crystal
Hydrogen bonds
$\pi-\pi$ interactions
Linear absorption
Fluorescence
Two-photon absorption

ABSTRACT

A new donor–bridge–acceptor (D–π–A) type ligand (**L**: 4′-(4-[4-(imidazole)styryl]phenyl)-2,2′:6′,2″-terpyridine) with two-photon absorption and coordination ability was designed and synthesized. Self-assembly of the ligand with HgX_2 (X = Cl, Br, I) yielded a series of new coordination complexes (**Dyes 1**–**3**) with five-coordinated mercury (II), which were characterized by single crystal X-ray diffraction determination. Solvent molecules and various weak interactions, including hydrogen bonds (C–H···N, C–H···X) and $\pi-\pi$ interactions played significant roles in the final topological structures. Linear and nonlinear optical properties of the ligand and three dyes were described. Experimental results revealed that two-photon absorption cross sections of three dyes are extraordinary stronger than that of ligand.

1. Introduction

Two-photon absorption (TPA) is a process in which two photons are simultaneously absorbed to an excited state in a medium *via* a virtual state under intense laser pulses when the sum of the energies of two absorbed photons matches well with the energy gap between an allowed excited state and the ground state. Since the theory was first proposed by Göppert-Mayer in 1931 [1], many researchers have been interested in seeking novel TPA materials due to their promising applications in optical limiting, two-photon laser scanning fluorescence imaging, microfabrication, 3D optical data storage, photodynamic therapy and so on [2]. They have done substantial research on structure–property relationships. Although it is still under exploration, thanks to the effort of scientists, some efficient molecular design strategies were put forward to provide guidelines for the development of materials with large TPA cross sections [3].

Scaling down these materials has recently afforded an exciting new class of highly tailorable organic–inorganic hybrids, which exhibits enhanced fluorescence and TPA activity by aggregation. The elegant work of Prasad [4] demonstrated that two-photon active dyes could be incorporated inside nanometer-sized silica nano-bubbles *via* a simple reverse micelle approach. The encapsulation of hydrophobic dyes within silica not only improves their water dispersibility but also leads to an increase in emission lifetime and efficiency as well as photostability. The studies of organic chromophores near the surface of silver nanoparticles with random fractal geometry or self-assembled ones on the nanoparticle surface exhibit large enhancement in two-photon activities relative to isolated chromophores [5,6].

Our group has developed a series of two-photon absorption materials [7] and modified nanoparticles [8]. Recently, a new series of organic–inorganic hybrid dyes had been reported to enhance the TPA and two-photon polymerization (TPP) properties *via* changing anions [9]. These results revealed that the packing and environment of the chromophores have profound influence on the TPA properties. Many TPA dyes reported based on conjugated aromatic rings are now available. Some complicated hetero-aromatic compounds are often used for special purposes in the two-photon area due to their favorable coordinate abilities. For example, 2, 2′:6′, 2″-terpyridine with a rigid framework plane and a superb ability to coordinate with various metal ions, is still not well explored [10,11].

* Corresponding author. Tel.: +86 551 5108151; fax: +86 551 5107342.
E-mail addresses: zhoufxfx@126.com, zhpzhp@263.net (H. Zhou).

0143-7208/$ – see front matter © 2011 Elsevier Ltd. All rights reserved.
doi:10.1016/j.dyepig.2011.03.024

Its derivatives are often used for many physical and chemical applications [12]. The recent success of the research on green and facile preparations of the key precursor 1,5-di(2-pyridinyl)-3-p-tolylpentane-1,5-dione (**3′**) [13] has aroused our interest in studying these derivatives from the two-photon materials point of view. By incorporating imidazolyl unit into the terpyridine backbone, a new D–π–A type compound, in which the terpyridyl ring is the acceptor part and an imidazolyl group as the donor one, was prepared (Fig. 1).

In this work, solvent-free Wittig reactions were used in building the π-conjugated system (Scheme 1). Our synthetic strategy is based on the molecular self-assembly of organic ligand with TPA properties and different inorganic salts. A series of new coordination complexes (**Dyes 1**–**3**) with five-coordinated mercury (II) were yielded by self-assembling the ligand with HgX_2 (X = Cl, Br, I), which were characterized by single crystal X-ray diffraction determination. Linear and nonlinear optical properties of the ligand and three dyes were investigated. Results showed these three new dyes exhibit enhanced TPA cross-section values, exceeding corresponding ligand, which offered a reference in designing and synthesizing new TPA materials with high performance.

2. Experimental section

2.1. Materials and physical measurements

Elemental analyses were performed with a Perkin–Elmer 240C elemental analyzer. The ^{1}H NMR spectra were recorded at 25 °C on a Bruker Avance 400 spectrometer, and the chemical shift are reported as parts per million (ppm) from TMS (δ). Coupling constants J are given in Hertz. Mass spectra were acquired on a Micromass GCT-MS (EI source). IR spectra were recorded on a NEXUS 870 (Nicolet) spectrophotometer in the 400–4000 cm^{-1} region using a powder sample on a KBr plate. UV–*vis* absorption spectra were recorded on a UV-3100 spectrophotometer. Fluorescence measurements were carried out using an Edinburgh FLS920 fluorescence spectrometer equipped with a 450W Xe lamp and a time-correlated single-photon counting (TCSPC) card. All the fluorescence spectra were collected. The single-photon excited fluorescence (SPEF) quantum yields (Φ) were measured by using a standard method under the same experimental conditions for all compounds. Rhodamine B dissolved in ethanol (Φ = 0.56) [14] at the same concentration as the other samples was used as the standard. The two-photon excited fluorescence (TPEF) spectra were measured using a mira 900-D Ti: sapphire femtosecond laser with a pulsewidth of 200 fs and a repetition rate of 76 MHz. All measurements were carried out in air at room temperature. TPA cross sections were measured using fluorescein as reference.

2.2. Materials and synthesis

All chemicals were available commercially, and the solvents were purified as conventional methods before use. These compounds were characterized by ^{1}H NMR, FT-IR, and MS spectrometry. Starting materials (**2′**–**6′**) were prepared according to literature procedures [15] (Scheme 1) and 4-(1H-Imidazol-1-yl)benzaldehyde was prepared according to literature procedures [16].

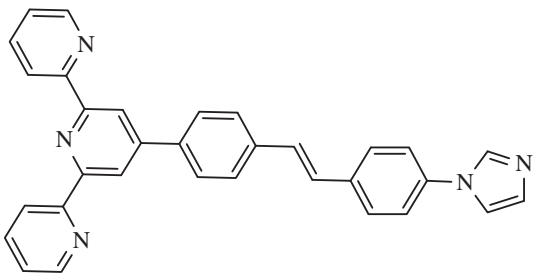

Fig. 1. Schematic drawing of the ligand (**L**).

2.2.1. Preparation of the ligand: 4′-(4-[4-(imidazolyl)styryl] phenyl)-2,2′:6′,2″-terpyridine

t-BuOK (1.38 g, 12.3 mmol) was placed into a dry mortar and well milled into powder, then **6′** (1.99 g, 3.0 mmol) and 4-(1H-Imidazol-1-yl)benzaldehyde (0.55 g, 3.2 mmol) were added and mixed. The mixture was milled vigorously for about 20 min. The mixture became sticky, and then tetrahydrofuran (5 mL) was added. The mixture was continuously milled for another 10 min. After completion of the reaction (monitored by Thin Layer chromatography (TLC)), the mixture was dispersed in 100 mL ethanol. The residual solid was filtered and recrystallized from anhydrous dichloromethane/ethanol, to give yellow crystals **L** (1.10 g, yield 76%). ^{1}H NMR ($CDCl_3$, 400 MHz): δ 7.17 (s, 1H), 7.45 (s, 2H), 7.53–7.56(m, 2H), 7.70–7.73 (d, J = 8.50 Hz, 2H), 7.81–7.84 (m, 4H), 7.86 (s, 1H), 7.98–8.00 (d, J = 8.30 Hz, 2H), 8.06–8.07 (m, 2H), 8.34 (s, 1H), 8.68–8.70 (d, J = 8.00 Hz, 2H), 8.76 (s, 2H), 8.78–8.79 (d, J = 4.51 Hz, 2H). MS: m/z (%) = 321.12 (100). FT-IR (KBr, cm^{-1}): 3408 (w), 3051 (w), 1584 (s), 1565 (s), 1466 (m), 1387 (s), 1242 (m), 1140 (m), 989 (m), 788 (s), 740 (s), 634 (m), 614 (m). Anal. Calcd for $C_{32}H_{23}N_5$: C, 80.48; H, 4.85; N, 14.66%. Found: C, 80.89; H, 4.50; N, 15.04%.

2.2.2. Preparation of dyes ***1***–***3***

$HgLCl_2 \cdot CHCl_3$(Dye 1): $HgCl_2$ (10.88 mg, 0.04 mmol) in 15 mL of MeOH was layered onto a solution of **L** (19.08 mg, 0.04 mmol) in 5 mL of $CHCl_3$ and stood for ten days to give yellow cube single crystals. Yield: 22 mg (73%). FT-IR (KBr, cm^{-1}): 3050 (w), 1595 (s), 1574 (s), 1521 (w), 1473 (m), 1401 (m), 1248 (m), 807 (s), 789 (s). Anal. Calcd for $C_{33}H_{24}Cl_5HgN_5$: C, 45.64; H, 2.79; N, 8.06%. Found: C, 45.19; H, 2.68; N, 7.65%.

$HgLBr_2 \cdot CHCl_3$(Dye 2): $HgBr_2$ (14.48 mg, 0.04 mmol) in 15 mL of MeOH was layered onto a solution of **L** (19.08 mg, 0.04 mmol) in 5 mL of $CHCl_3$ and stood for ten days to give yellow cube single crystals. Yield: 24 mg (72%). FT-IR (KBr, cm^{-1}): 3057 (w), 1596 (s), 1573 (s), 1522 (w), 1475 (m), 1400 (m), 1247 (m), 807 (s), 789 (s). Anal. Calcd for $C_{33}H_{24}Br_2Cl_3HgN_5$: C, 41.40; H, 2.53; N, 7.32%. Found: C, 41.06; H, 2.44; N, 7.08%.

$HgLI_2 \cdot CHCl_3$(Dye 3): HgI_2 (18.24 mg, 0.04 mmol) in 15 mL of MeOH was layered onto a solution of **L** (19.08 mg, 0.04 mmol) in 5 mL of $CHCl_3$ and stood for ten days to give yellow cube single crystals. Yield: 29 mg (78%). FT-IR (KBr, cm^{-1}): 3055 (w), 1595 (s), 1541 (s), 1521 (w), 1475 (m), 1399 (m), 1246 (m), 807 (s), 788 (s). Anal. Calcd for $C_{33}H_{24}Cl_3HgI_2N_5$: C, 37.70; H, 2.30; N, 6.66%. Found: C, 37.33; H, 2.27; N, 6.31%.

2.3. X-ray crystallography

X-ray diffraction data of single crystals were collected on a Siemens Smart 1000 CCD diffractometer. The determination of unit cell parameters and data collections were performed with Mo Kα radiation (λ = 0.71073 Å). Unit cell dimensions were obtained with least-squares refinements, and all structures were solved by direct methods using SHELXS-97 [17]. The other non-hydrogen atoms were located in successive difference Fourier syntheses. The final refinement was performed by using full-matrix least-squares methods with anisotropic thermal parameters for non-hydrogen atoms on F^2. The hydrogen atoms were added theoretically and riding on the concerned atoms. Crystallographic crystal data and

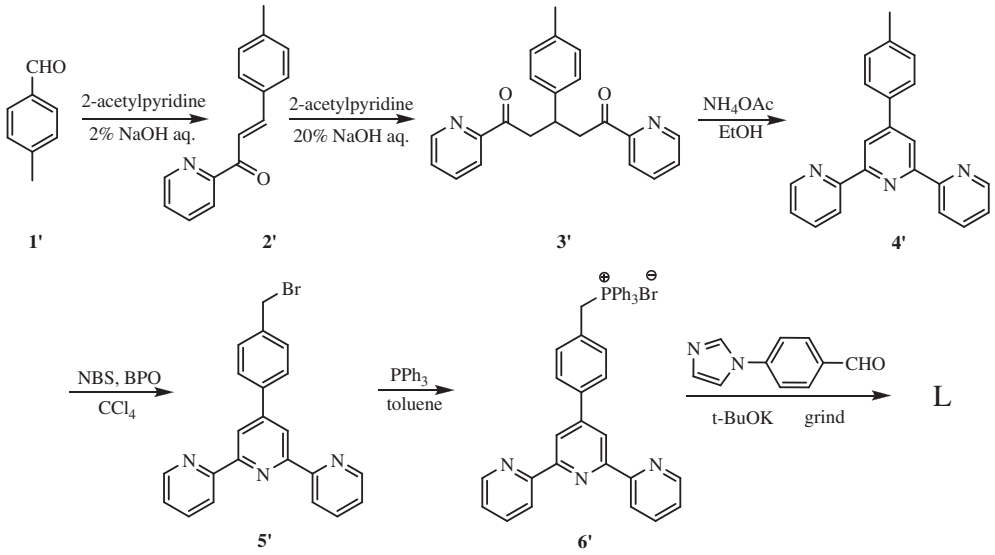

Scheme 1. Synthesis strategy for the preparation of **L**.

processing parameters for dyes **1**–**3** are shown in Table 1. Selected bond lengths and bond angles for dyes **1**–**3** are listed in Table 2.

3. Results and discussion

3.1. Structure of dyes *1*–*3*

3.1.1. Structure of $HgLCl_2 \cdot CHCl_3$ (dye *1*)

Dye **1** crystallizes in the monoclinic form with space group *C*2/c as shown in Fig. 2a. The unit consists of one mercury ion connecting three N from one **L** and two chlorine atoms, and a free solvent chloroform molecule. The bond lengths Hg1–N1, Hg1–N2, Hg1–N3 are 2.400(8), 2.403(7), 2.441(9) Å, respectively. Each bond angle around the mercury atom is in the range 68.2(3)–133.4(3)°, indicating a quite distorted tetrahedral geometry. Selected bond lengths and angles are listed in Table 2. Besides, the chloroform molecule connects to mercury salt through C–H···Cl hydrogen bonds (the chloroform molecule provided H and mercury salt provided Cl, d(H34···Cl2) = 2.659 Å and ∠(C34–H34···Cl1) = 153.24°).

As shown in Fig. 2b, the imidazole ring does not directly involve in coordination, but the lone pair electrons from the N atom still have a strong Pro-e-competence, which generates a 1-D chain along *c*-axis through C–H···N bond interactions (rose dashed line, d(C4–H4···N4) = 2.689 Å, yellow dashed line, d(C17–H17···N4) = 2.694 Å, the angle of C4–H4–N4 is 155.15° and the angle of C17–H17–N4 is 166.27°). Also it can be seen that there are $\pi-\pi$ stacking contacts (red dashed line) with the shortest distance to be 3.470 Å between two neighboring dimers. Extraordinarily, the chloroform molecules play the vital role in the dimmer formation (pink dashed line, d(C34–H34···Cl2) = 2.659 Å and the angle of C34–H34···Cl2 is 153.23°, sky blue dashed line, d(Cl1···Cl5) = 3.236 Å, and the van der waals radii of H and Cl atom are 1.20 and 1.80 Å,).

Table 1
Crystallographic data for dyes **1**–**3**.

Compound	Dye **1**	Dye **2**	Dye **3**
Empirical formula	$C_{32}H_{23}Cl_2HgN_5$	$C_{32}H_{23}Br_2HgN_5$	$C_{32}H_{23}I_2HgN_5$
Formula weight	868.41	957.33	1051.31
Crystal system	Monoclinic	Monoclinic	Monoclinic
Space group	C2/c	C2/c	C2/c
a [Å]	21.220(5)	21.280(5)	21.476(5)
b [Å]	17.455(5)	17.438(5)	17.520(5)
c [Å]	17.578(5)	17.597(5)	17.983(5)
α[°]	90.000(5)	90.000(5)	90.000(5)
β[°]	94.353(5)	92.899(5)	92.016(5)
γ[°]	90.000(5)	90.000(5)	90.000(5)
V [Å^3]	6492(3)	6522(3)	6762(3)
Z	8	8	8
T [K]	298(2)	298(2)	298(2)
D_{calcd}[g cm^{-3}]	1.777	1.950	2.065
μ [mm^{-1}]	5.186	7.449	6.647
θrange [°]	1.51–25.00	1.51–25.00	1.50–24.99
Total no. data	5684	5757	5970
No. unique data	3029	3072	3729
No. params refined	398	397	397
R_1	0.0523	0.0522	0.0458
wR_2	0.1258	0.1333	0.1252
GOF	1.034	0.958	0.930

Table 2
Selected bond lengths (Å) and angles (°) for dyes **1**–**3**.

Dye **1**			
Hg1–N1	2.400(8)	Cl1–Hg1–Cl2	118.27(12)
Hg1–N2	2.403(7)	Cl1– Hg1–N1	105.0(2)
Hg1–N3	2.441(9)	Cl1–Hg1–N2	109.89(19)
Hg1–Cl1	2.428(3)	Cl1–Hg1–N3	99.5(2)
Hg1–Cl2	2.425(3)	Cl2–Hg1–N1	104.1(2)
N1–Hg1–N2	68.2(3)	Cl2–Hg1–N2	131.3(2)
N1–Hg1–N3	133.4(3)	Cl2–Hg1–N3	98.1(2)
Dye **2**			
Hg1–N1	2.402(9)	Br1–Hg1–Br2	117.97(5)
Hg1–N2	2.391(8)	Br1–Hg1–N1	103.2(2)
Hg1–N3	2.447(10)	Br1–Hg1–N2	131.6(2)
Hg1–Br1	2.5431(15)	Br1–Hg1–N3	98.5(2)
Hg1–Br2	2.5496(17)	Br2–Hg1–N1	107.0(2)
N1–Hg1–N2	67.4(3)	Br2–Hg1–N2	109.9(2)
N1–Hg1–N3	131.8(3)	Br2–Hg1–N3	99.6(3)
Dye **3**			
Hg1–N1	2.483(9)	I1–Hg1–I2	120.95(3)
Hg1–N2	2.434(8)	I1–Hg1–N1	97.7(2)
Hg1–N3	2.429(8)	I1–Hg1–N2	108.2(2)
Hg1–I1	2.7128(11)	I1–Hg1–N3	108.9(2)
Hg1–I2	2.6993(11)	I2–Hg1–N1	98.8(2)
N1–Hg1–N2	66.1(3)	I2–Hg1–N2	130.3(2)
N1–Hg1–N3	131.2(3)	I2–Hg1–N3	101.15(19)

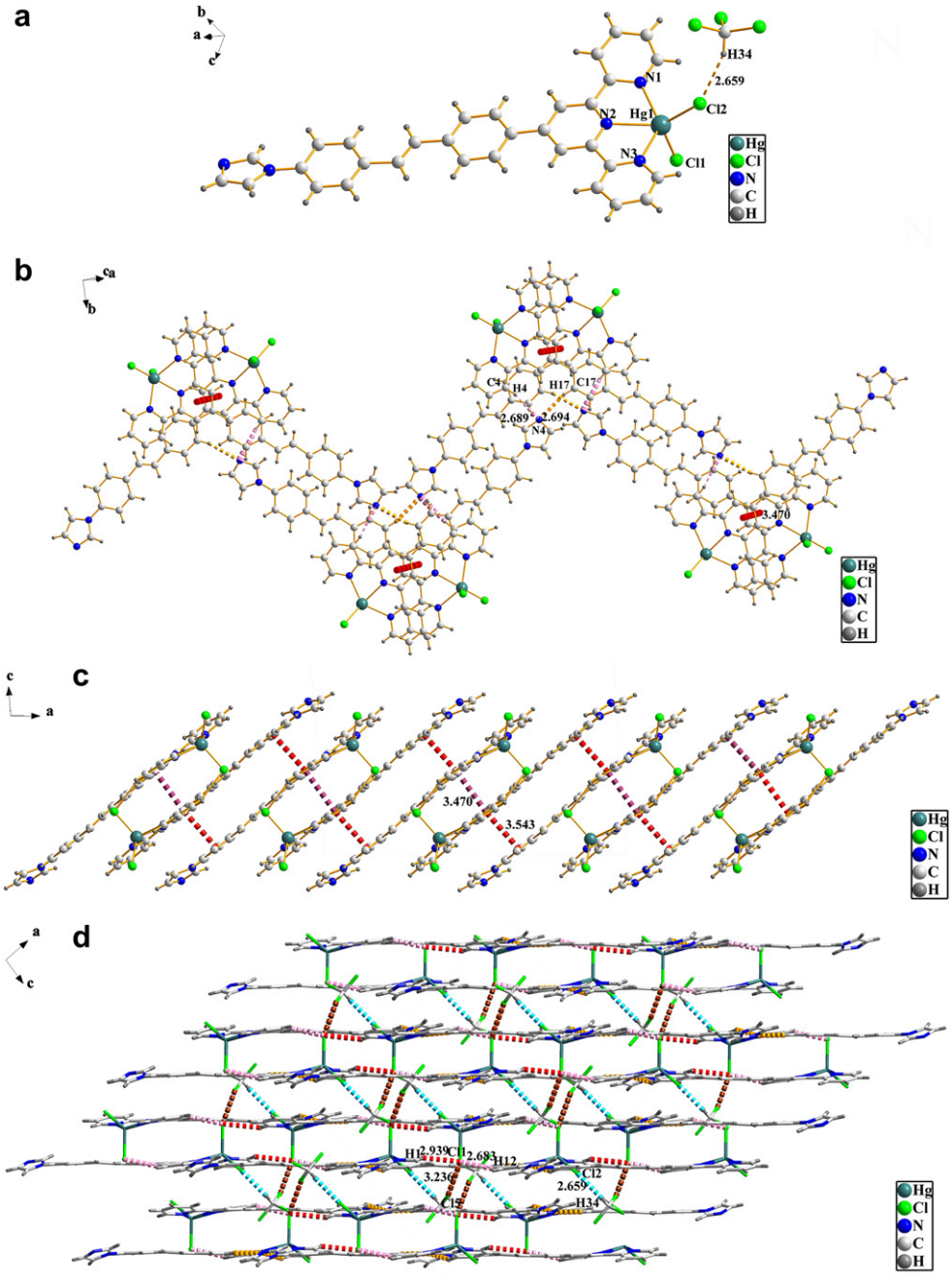

Fig. 2. (a) Coordination environments of Hg with the atom numbering scheme. (b) The 1-D framework of dye 1 showing the C–H···N (rose and yellow) hydrogen bond and $\pi-\pi$ stacking (red) along the *c*-axis. (c) The 2-D framework of dye 1 showing $\pi-\pi$ stacking along the *a*-axis. (d) The 3-D architecture of dye 1 showing the C–H···Cl (red and rose) hydrogen bond along the *b*-axis. (For interpretation of the references to color in this figure legend, the reader is referred to the web version of this article.)

From Fig. 2c, dye **1** formed a 2-D framework through $\pi-\pi$ stacking interactions (red dashed line, the shortest distance is 3.543 Å, plum dashed line, the shortest distance is 3.470 Å) between the neighboring dimers along *a*-axis.

Finally, the extended 3-D topological structures are formed along the *b*-axis *via* C–H···Cl interactions (red dashed line, d(C1–H1···Cl1) = 2.939 Å, d(C12–H12···Cl1) = 2.683 Å, the angle of C1–H1–Cl1 is 131.87° and the angle of C12–H12–Cl1 is 154.75°) (Fig. 2d).

3.1.2. Structure of $HgLBr_2 \cdot CHCl_3$ (Dye **2**)

Similar to dye **1**, dye **2** also indicates a quite distorted tetrahedral geometry, which consists of one mercury (II) connecting three N from **L**, two bromine atoms and one chloroform molecule. The X-ray single crystal reveals that dye **2** also crystallizes in the monoclinic form with space group C2/c as shown in Fig. 3a. The bond lengths Hg1–N1, Hg1–N2, Hg1–N3 are 2.402, 2.391, 2.447 Å, respectively. Each bond angle around the mercury atom is in the range 65.9(3)–131.8(3)°. Selected bond lengths and angles are listed in Table 2. However, different from dye **1**, the chloroform molecule connects to the ligand through C–H···Cl hydrogen bonds (the chloroform molecule provided Cl and the ligand provided H, d(H25···Cl2) = 2.671 Å and ∠(C25–H25···Cl2) = 160.21°).

Fig. 3b shows that the weak force of C–H···Br is widely spread in the complex to construct this super molecular structure. Also we can find that the chloroform molecules play a very important role

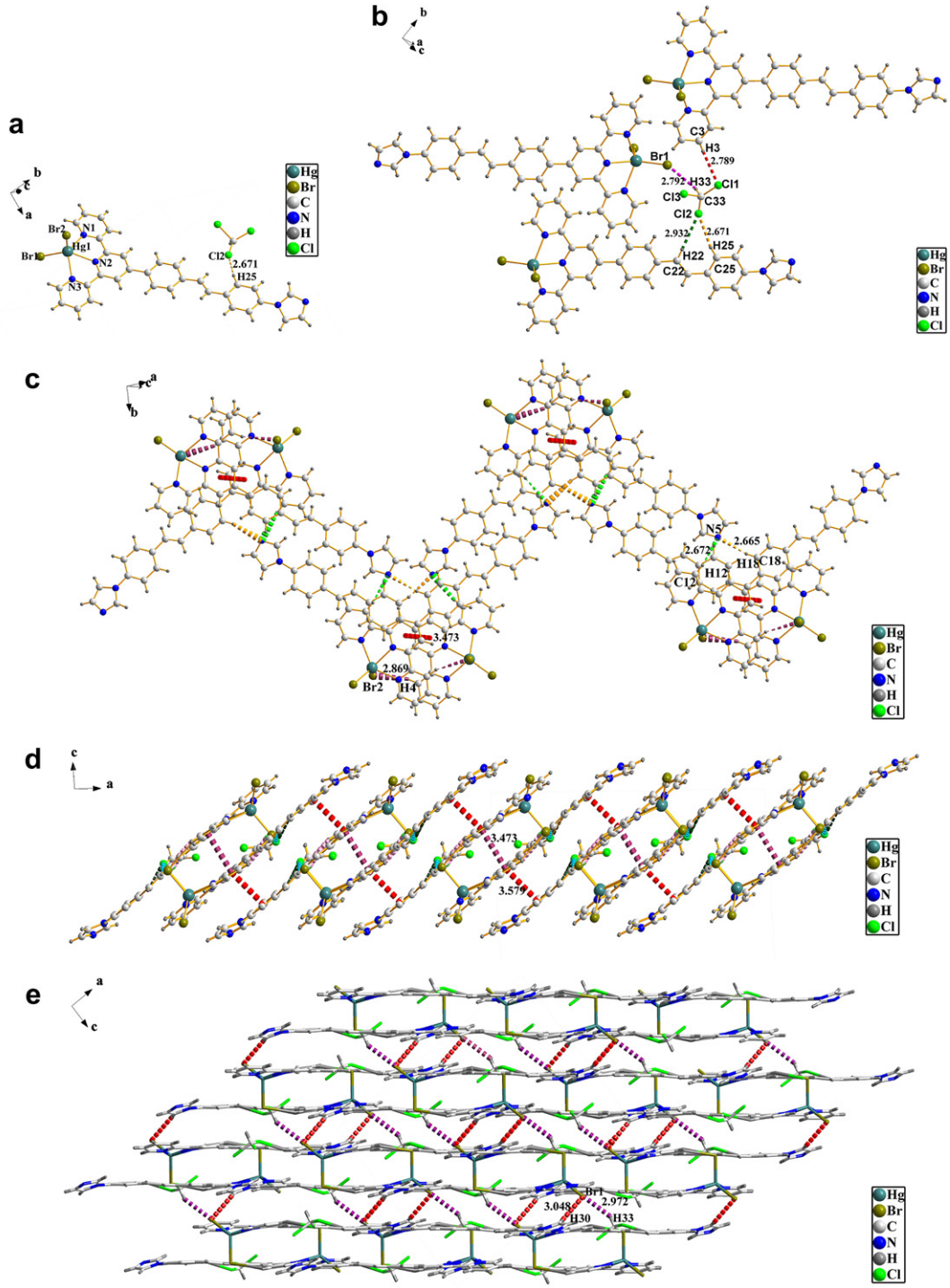

Fig. 3. (a) Coordination environments of Hg with the atom numbering scheme. (b) Weak interactions form solvent in dye **2**. (c) The 1-D framework of dye **2** showing the C–H···N (green and light orange) hydrogen bond and $\pi-\pi$ stacking (red) along the *c*-axis. (d) The 2-D framework of dye **2** showing $\pi-\pi$ stacking along the *a*-axis. (e) The 3-D architecture of dye **2** showing the C–H···Br (red and pink) hydrogen bond along the *b*-axis. (For interpretation of the references to color in this figure legend, the reader is referred to the web version of this article.)

as follows: (1)Cl2 and C22, H22, C25, H25 of dye form of C–H···Cl bonds (green dashed line, d(C22–H22···Cl2) = 2.932 Å, light orange dashed line, d(H25···Cl2) = 2.671 Å, the angle of C22–H22–Cl2 is 174.62° and the angle of C25–H25–Cl2 is 160.21°). (2) Cl1 and C3, H3 of dye form of C–H···Cl bond with the distance of C3–H3···Cl1 is 2.798 Å (red dashed line) and the angle of C3–H3–Cl1 is 160.67°. (3) Br1 and C33, H33 of dye form of C–H···Br bond with the distance of C33–H33···Br1 is 2.971 Å (rose dashed line) and the angle of C33–H33–Br1 is 150.94°.

Similar to dye **1**, dye **2** generates a 1-D chain along *c*-axis through C–H···N bond interactions (bright green dashed line, d(C12–H12···N5) = 2.672 Å, light orange dashed line, d(C18–H18···N5) = 2.665 Å, the angle of C12–H12–N5 is 155.72° and the angle of C18–H18–N5 is 167.40°). Also it can be seen that

there are $\pi-\pi$ stacking interactions (red dashed line, the shortest distance is 3.473 Å) between two neighboring dimmers (Fig. 3c).

From Fig. 3d, dye **2** forms a 2-D framework through $\pi-\pi$ stacking (red dashed line, the shortest distance is 3.579 Å, plum dashed line, the shortest distance is 3.473 Å) between the neighboring dimers along a-axis.

Finally, dye **2** forms a stable 3-D architecture through C–H···Br interactions (red dashed line, d(C30–H30···Br1) = 3.048 Å, pink dashed line, d(C33–H33···Br1) = 2.972 Å, the angle of C30–H30–Br1 is 142.78° and the angle of C33–H33–Br1 is 150.93°) along *b*-axis (Fig. 3e).

3.1.3. Structure of $HgLI_2 \cdot CHCl_3$ (Dye **3**)

Dye **3** adopts the same coordination mode as dye **2**. The single crystal analysis of dye **3** reveals that the mercury (II) is five-coordinated *via* three N atoms from **L** and two I atoms. The bond lengths Hg1–N1, Hg1–N2, Hg1–N3 are 2.483, 2.434, 2.429 Å, respectively (Fig. 4a). Each bond angle around the mercury atom is in the range

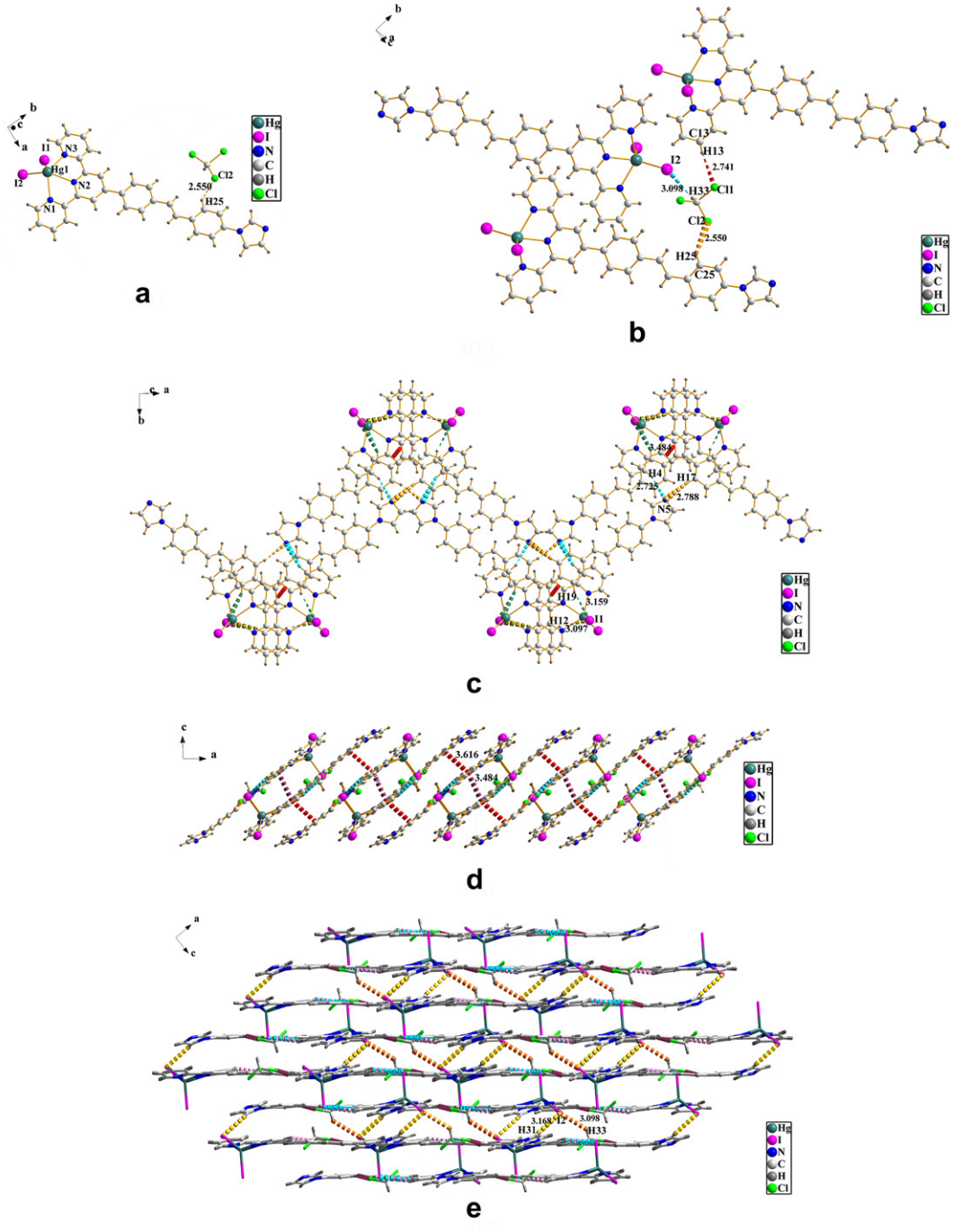

Fig. 4. (a) Coordination environments of Hg with the atom numbering scheme. (b) Weak interactions form solvent in dye **3**. (c) The 1-D framework of dye **3** showing the C–H···N (turquoise and light orange) hydrogen bond, the C–H···I (dark yellow and sea green) hydrogen bond and $\pi-\pi$ stacking (red) along the *c*-axis. (d) The 2-D framework of dye **3** showing $\pi-\pi$ stacking along the *a*-axis. (e) The 3-D architecture of dye **3** showing the C–H···I (gold and orange) hydrogen bond along the *b*-axis. (For interpretation of the references to color in this figure legend, the reader is referred to the web version of this article.)

Table 3
Photophysical properties of **L**, **Dye 1**, **Dye 2** and **Dye 3** in several of different polar solvents.

Cmpd	Solvents	Benzene	Ethyl acetate acetate	THF	Ethanol	Acetonitrile	DMF
L	λ/nm[a]	282, 333	283, 331	283, 331	283, 332	281, 333	284, 334
	λ/nm[b]	390, 410	409	414	422	424	434
	Φ^c	0.11	0.07	0.09	0.06	0.07	0.11
	Δν/cm^{-1}[d]	5640	5762	6057	6424	6445	6899
Dye 1	λ/nm[a]	281, 328	282, 326	282, 331	283, 327	282, 328	281, 334
	λ/nm[b]	391, 410	409	412	422	424	432
	Φ^c	0.12	0.07	0.07	0.05	0.08	0.10
	Δν/cm^{-1}[d]	6098	6225	5940	6884	6903	6792
Dye 2	λ/nm[a]	282, 327	275, 323	278, 331	285, 326	275, 327	279, 335
	λ/nm[b]	391, 410	408	413	424	424	434
	Φ^c	0.19	0.08	0.09	0.08	0.10	0.11
	Δν/cm^{-1}[d]	6191	6450	5999	7090	6996	6809
Dye 3	λ/nm[a]	279, 328	275, 324	278, 331	280, 325	275, 322	283, 331
	λ/nm[b]	391, 410	407	414	423	425	433
	Φ^c	0.18	0.09	0.09	0.07	0.08	0.11
	Δν/cm^{-1}[d]	6098	6294	6057	7129	7526	7117

[a] Peak position of the longest absorption band.
[b] Peak position of SPEF, exited at the absorption maximum.
[c] Quantum yields determined by using coumarin as standard.
[d] Stokes' shift in cm^{-1}.

66.1(3)–131.2(3)°, indicating a quite distorted tetrahedral geometry. Selected bond lengths and angles are listed in Table 2. Similar to dye **2**, both the chloroform molecules and π–π stacking between two neighboring dimmers play a significant role in 1-D and 2-D framework, as well as C–H···I interactions.

From the crystal structures of three dyes, the five-coordination mode of Hg (II) with a quite distorted tetrahedral geometry is very interesting, which is different from the most common coordination framework of mercury atoms that is four-coordination and six-coordination [18]. In our dyes, the Hg atoms are all five-coordination, which is probably due to the specific structure of the ligand for its good planarity. Meanwhile, the nitrogen atoms distribute evenly on the rings, which is advantageous in forming the spatial structure of the distorted tetrahedron.

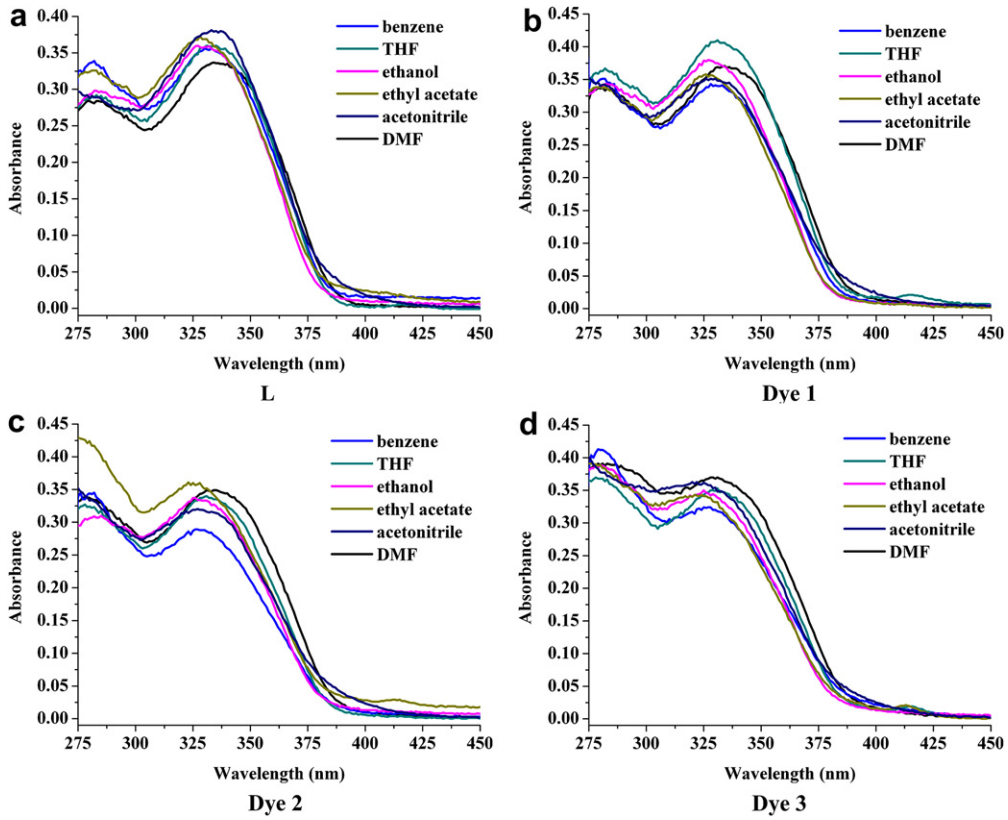

Fig. 5. Linear absorption spectra of **L**, dye 1, dye **2** and dye **3** in six solvents.

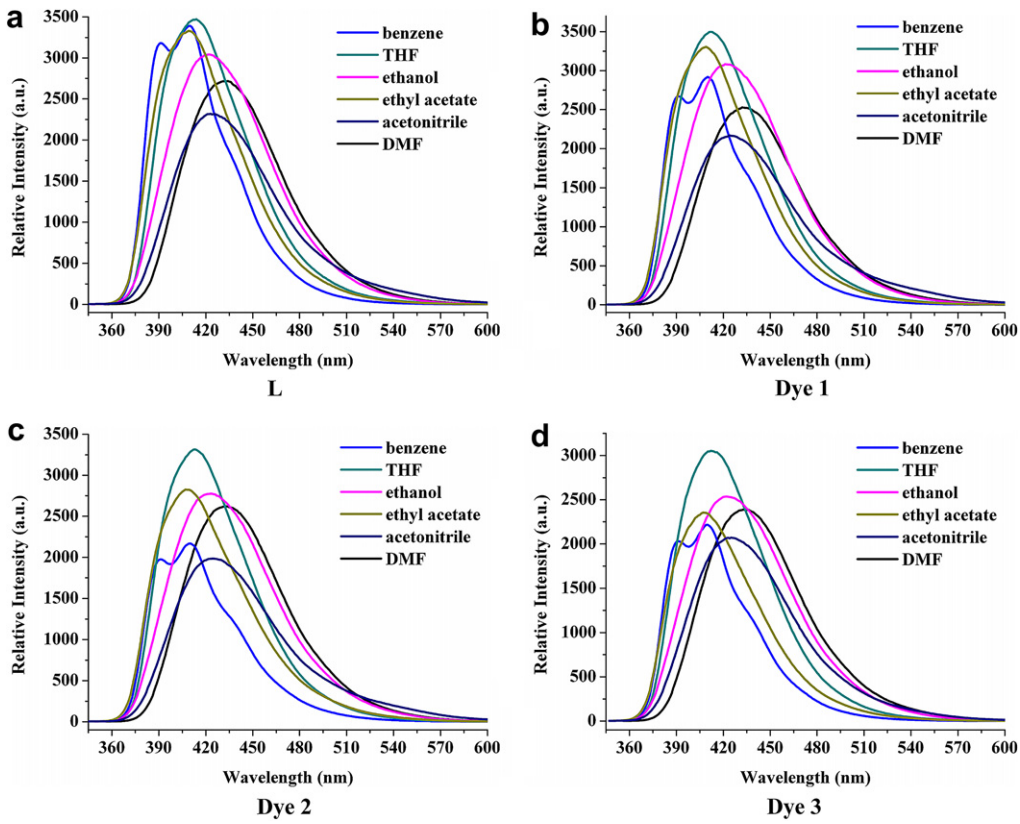

Fig. 6. The one-photon fluorescence spectra of **L**, dye 1, dye **2** and dye **3**.

4. Linear absorption and single-photon excited fluorescence (SPEF)

The photophysical properties (absorption and fluorescence) of the new series of dyes in six different solvents are collected in Table 3 including fluorescence quantum yields.

4.1. Absorption properties

Linear absorption spectra of **L**, dye **1**, dye **2** and dye **3** in benzene, ethyl acetate, THF, ethanol, acetonitrile and DMF with a solution concentration of $c = 1.0 \times 10^{-5}$ mol/L are shown in Fig. 5. From Table 3, one can observe that each of their absorption spectra exhibits two peaks between 250 nm and 400 nm and the absorption maxima of **L** and three dyes are located at 334, 334, 335 and 331 nm in DMF, respectively, which corresponds to the π–π^* transition of the main chain. The absorption spectrum is not very sensitive to the solvent polarity. The linear absorption spectra of **L** and three dyes in six different solvents are shown in Fig. 5 and one can observe that there is no linear absorption in the entire spectral range from 450 to 900 nm.

4.2. Fluorescence properties

The SPEF spectra were measured at the same concentration as that of the linear absorption spectra. As shown in Fig. 6 and Table 3, the SPEF spectra of **L**, dye **1**, dye **2** and dye **3** display pronounced positive solvatochromism (i.e., bathochromic shift with increasing solvent polarity) in their emission spectra. The emission maxima of **L** and dyes are about 410 nm in benzene. In high polar solvent DMF, the peak is located at 434 nm, which is red-shifted by 24 nm due to the different molecular environment. Large values of the Stokes shift are observed for **L** and three dyes in six solvents due to strong solvent-solute dipole–dipole interactions, a manifestation of the large dipole moment and orientational polarizability. Because **L** and three dyes contain an electron-donating group and an electron-withdrawing group, they exhibit a significant dipole moment in the ground state, which depends on charge separation in the fluorophore. In the excited state, it is likely that this charge separation increases, resulting in a larger dipole moment than that in the ground state [19]. Thus, such an increase in dipole moment would explain the sensitivity of the emission spectra of these dipolar compounds to solvent polarity. Besides, the fluorescence intensity of **L** decreases gradually with increasing solvent polarity. From Fig. 6, the two peaks phenomenon in the minimum polar solvent of benzene, has been observed, which may be attributes to the twisted intramolecular charge transfer (TICT) [20]. The quantum yields (Φ)

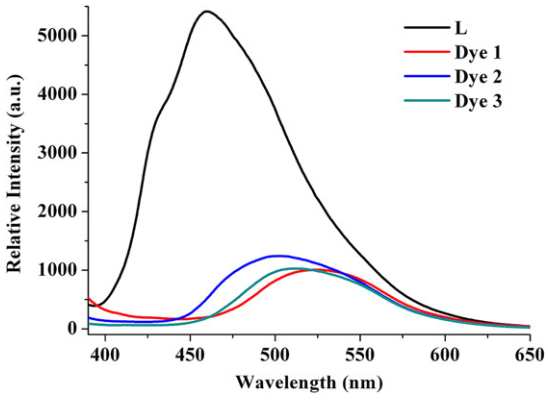

Fig. 7. The Solid-State fluorescence spectra of **L**, dye 1, dye 2 and dye 3.

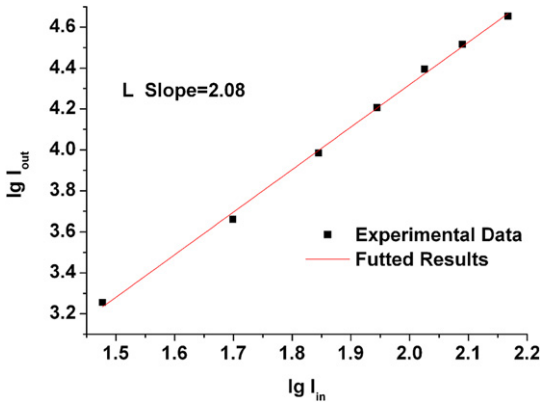

Fig. 8. Output fluorescence (I_{out}) vs. the square of input laser power (I_{in}) for **L**. Excitation carried out at 720 nm, with $c = 1.0 \times 10^{-3}$ mol/L in DMF.

of the ligand and the three complexes in different solvents are determined by using RhB as a standard. Upon increasing the solvent polarity, the fluorescence quantum yields exhibit no obvious decrease. This behavior is different from previous reports [21].

As shown in Fig. 7, the Solid-State fluorescence maxima of **L** locates at 460 nm and three coordination complexes dye **1**, **2** and **3** locate at 526, 503 and 511 nm, respectively. The Solid-State fluorescence spectrum shows a marked red shift of the maximum corresponding to the metal to ligand charge transfer (MLCT) transition upon coordination **L** with Hg (II) salts.

4.3. Two-photon excited fluorescence (TPEF)

There is no linear absorption in the wavelength range 450–850 nm for the ligand and the three complexes, which indicates that there are no molecular energy levels corresponding to an electron transition in the spectral range. Therefore, upon excitation from 450 to 850 nm, it is impossible to produce single-photon excited up-converted fluorescence. If frequency up-converted fluorescence induced with a laser in this spectral range appears, it can be ascribed to two-photon excited fluorescence (TPEF). Fig. 8 shows a log–log plot of the excited fluorescence signal versus excited light power. It provides direct evidence for the squared dependence of excited fluorescence power and input laser intensity.

As shown in Fig. 9, the TPA spectra of **L** and dye **1** are determined in the wavelength range by investigating their two-photon excited fluorescence (TPEF) in DMF with a concentration of 1.0×10^{-3} mol/L. The TPA spectra of dye **2** and dye **3** are similar to that of dye **1**. The absorption maxima locate at 448 and 487 nm for **L**, 526 nm for dye **1**, dye **2** and dye **3** in DMF, respectively.

The TPA cross sections (δ) are determined by comparing their TPEF to that of fluorescein in DMF, according to the following equation [22]:

$$\delta = \delta_{ref}\frac{\Phi_{ref}}{\Phi}\frac{c_{ref}}{c}\frac{n_{ref}}{n}\frac{F}{F_{ref}}$$

Here, the subscripts ref. stands for the reference molecule. δ is the TPA cross-section value, c is the concentration of solution, n is the refractive index of the solution, F is the TPEF integral intensities of the solution emitted at the exciting wavelength, and Φ is the fluorescence quantum yield. The δ_{ref} value of reference was taken from the literature [23].

Detailed experiments reveal that from 715 to 830 nm, the peak position in the TPEF spectra of these complexes is independent of the excitation wavelength, but the TPA cross sections are dependent over this range. By tuning the pump wavelength incrementally from 715 to 830 nm while keeping the input power fixed and then recording the TPEF intensity, the two-photon absorption spectra

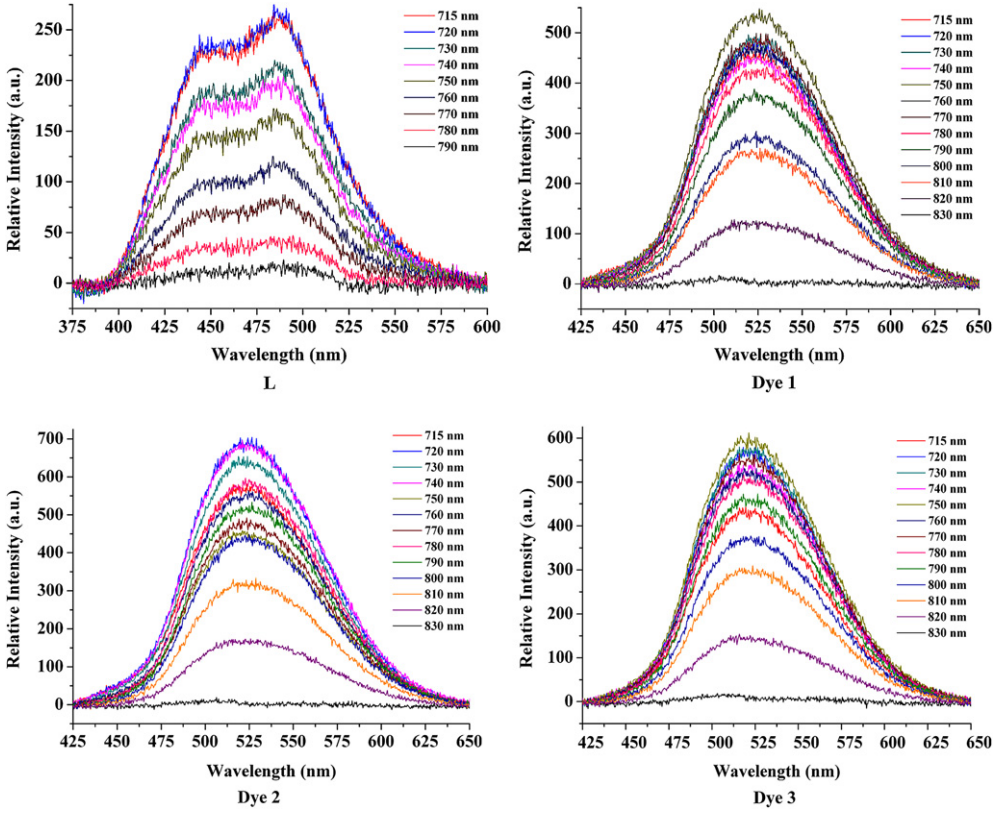

Fig. 9. The TPA spectra of **L**, dye **1**, dye **2** and dye **3** in DMF under different excitation wavelengths.

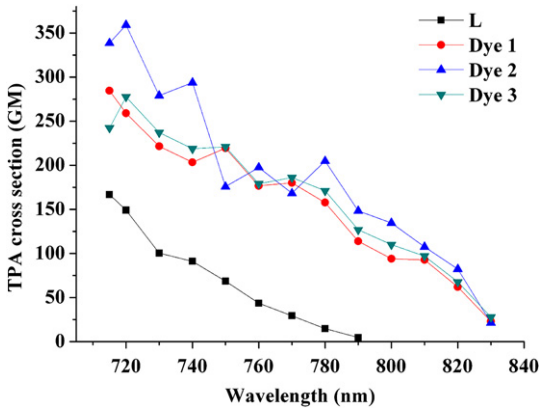

Fig. 10. Two-photon (from a 200 fs, 76 MHz, Ti: sapphire laser) absorption cross sections of **L**, dye **1**, dye **2** and dye **3** in DMF versus excitation wavelengths of identical energy of 0.100 w. (experimental uncertainties: 10%)

are obtained. By referencing the TPA cross section of fluorescein to be 19 GM (1 GM = 10^{-50} cm^{-4} s $photon^{-1}$) [24], the maximum two-photon absorption cross sections of complexes are 149 GM for **L**, 259 GM for dye **1**, 359 GM for dye **2** and 278 GM for dye **3** in DMF at 720 nm.

Fig. 10 shows the TPA action spectrum of **L**, **L**–**Hg (II)** in the 715–830 nm range. It has been found that two-photon absorption cross sections of **L**–**Hg (II)** from 715 to 830 nm are always larger than that of **L,** which is unusual for Hg complexes. The behavior observed here in the TPA spectra, can be attributed to the enlarged conjugation length upon Hg (II) addition **L**, a new D–π–A type compound, in which the terpyridyl ring is the acceptor part and an imidazolyl group is the donor one. When **L** is coordinated with HgX_2, the Hg^{2+} becomes the acceptor, which induces a larger localization of the electrons. The Solid-State Two-photon excited fluorescence spectra further testify it, in which red shift is obviously observed in the emission spectra of three dyes comparing with the ligand. But in 10^{-5} dilute solution, the emission spectra of three dyes and the ligand are almost the same, which can be induced by ionization of Hg (II) complexes.

5. Conclusions

In summary, a series of new coordination complexes (dyes **1**–**3)** are synthesized by self-assembly of the new ligand 4′-(4-[4-(imidazolyl)styryl]phenyl)-2, 2′: 6′, 2″-terpyridine with HgX_2 (X = I, Br, Cl). Solvent molecules and various weak interactions, including hydrogen bonds (C–H···N, C–H···X) and π–π contacts play significant roles in the final topological structures. Surprisingly, TPA-induced fluorescence of **L**–**Hg (II)** at 720 nm is obviously stronger than that of **L**, which can be ascribed to the enlarged conjugation length when Hg^{2+} becomes the acceptor.

Acknowledgments

This work was supported by a grant for the National Natural Science Foundation of China (21071001, 50873001), Education committee of Anhui Province (KJ2009A52, KJ2010A030), The team for scientific Innovation Foundation of Anhui Province (2006KJ007TD), Science and Technological Fund of Anhui Province for Outstanding Youth (10040606Y22), The 211 Project of Anhui University, National university student innovation test plan (091035707), Ministry of education funded projects focus on retured overseas scholar.

Appendix. Supplementary material

Supplementary material associated with the article can be found in online version, at doi:10.1016/j.dyepig.2011.03.024.

References

[1] Göppert-Mayer M. Annals of Physics (Leipzig) 1931;9:273.
[2](a) Cumpston BH, Ananthavel SP, Barlow S, Dyer DL, Ehrlich JE, Erskine LL, et al. Two-photon polymerization initiators for three-dimensional optical data storage and microfabrication. Nature 1999;398:51–4;
(b) Bouit PA, Wetzel G, Berginc G, Loiseaux B, Toupet L, Feneyrou P, et al. Near IR nonlinear absorbing chromophores with optical limiting properties at telecommunication wavelengths. Chemistry of Materials 2007;19:5325–35;
(c) Kawata S, Sun HB, Tanaka T, Takada K. Finer features for functional microdevices. Nature 2001;412:697–8;
(d) He GS, Bhawalkar JD, Zhao CF, Prasad PN. Optical limiting effect in a two-photon absorption dye doped solid matrix. Applied Physics Letters 1995;67:2433–5;
(e) Kim HM, Jung C, Kim BR, Jung SY, Hong JH, Ko YG, et al. Environment-sensitive two-photon probe for tntracellular free magnesium ions in live tissue. Angewandte Chemie International Edition 2007;46:3460–3;
(f) He GS, Tan LS, Zheng QD, Prasad PN. Near IR nonlinear absorbing chromophores with optical limiting properties at telecommunication wavelengths. Chemical Reviews 2008;108:1245–330;
(g) Kim HM, Cho BR. Two-photon materials with large two-photon cross sections. Structure–property relationship. Chemical Communications 2009;2:153–64;
(h) Gao YH, Wu JY, Li YM, Sun PP, Zhou HP, Yang JX, et al. A sulfur-terminal Zn(II) complex and its two-photon microscopy biological imaging application. Journal of the American Chemical Society 2009;131:5208–13.
[3](a) Beljonne D, Wenseleers W, Zojer E, Shuai Z, Vogel H, Pond SJK, et al. Role of dimensionality on the two-photon absorption response of conjugated molecules: the case of octupolar compounds. Advanced Functional Materials 2002;12:631–41;
(b) Bartholomew GP, Ledoux I, Mukamel S, Bazan GC, Zyss J. Three-dimensional nonlinear optical chromophores based on through-space delocalization. Journal of the American Chemical Society 2002;124:13480–5;
(c) Mongin O, Porrés L, Charlot M, Katan C, Blanchard-Desce M. Synthesis, fluorescence, and two-photon absorption of a series of elongated rodlike and banana-shaped quadrupolar fluorophores: a comprehensive study of structure–property relationships. Chemical A European Journal 2007;13:1481–98;
(d) Zheng QD, He GS, Prasad PN. π-conjugated dendritic nanosized chromophore with enhanced two-photon absorption. Chemistry of Materials 2005;17:6004–11;
(e) Tian YP, Li L, Zhou YH, Wang P, Zhou HP, Wu JY, et al. Design and synthesis of two New two-photon absorbing pyridine salts as ligands and their rare earth complexes. Crystal Growth and Design 2009;9:1499–504;
(f) Kim HM, Kim BR, An MJ, Hong JH, Lee KJ, Cho BR. Two-photon fluorescent probes for long-term imaging of calcium waves in live tissue. Chemical A European Journal 2008;14:2075–83;
(g) Tian N, Xu QH. Enhanced two-photon excitation fluorescence by fluorescence resonance energy transfer using conjugated polymers. Advanced Materials 2007;19:1988–91;
(h) Wang B, Wang YC, Hua JL, Jiang YH, Huang JH, Qian SX, et al. Starburst triarylamine donor–acceptor–donor quadrupolar derivatives based on cyano-substituted biphenylaminestyryl-benzene: tunable aggregation-induced emission colors and large two-photon absorption cross sections. Chemical A European Journal 2011;17:2647–55;
(i) Jiang YH, Wang YC, Hua JL, Tang J, Li B, Qian SX, et al. Multibranched triarylamine end-capped triazines with aggregationinduced emission and large two-photon absorption cross-sections. Chemical Communications 2010;46:4689–91.
[4](a) Lal M, Levy L, Kim KS, He GS, Wang X, Min YH, et al. Silica nanobubbles containing an organic dye in a multilayered organic/inorganic heterostructure with enhanced luminescence. Chemistry of Materials 2000;12:2632–9;
(b) He GS, Zheng QD, Yong KT, Erogbogbo F, Swihart MT, Prasad PN. Two- and three-photon absorption and frequency upconverted emission of silicon quantum dots. Nano Letters 2008;8:2688–92.
[5] Wenseleers W, Stellacci F, Meyer-Friedrichsen T, Mangel T, Bauer CA, Pond SJK, et al. Five orders-of-magnitude enhancement of two-photon absorption for dyes on silver nanoparticle fractal clusters. Journal of Physical Chemistry B 2002;106:6853–63.
[6](a) Stellacci F, Bauer CA, Meyer-Friedrichsen T, Wenseleers W, Marder SR, Perry JW. Ultrabright supramolecular Beacons based on the self-assembly of two-photon chromophores on metal nanoparticles. Journal of the American Chemical Society 2003;125:328–9;
(b) Varnavski OP, Ranasinghe M, Yan X, Bauer CA, Chung SJ, Perry JW, et al. Ultrafast energy migration in chromophore shell–metal nanoparticle

assemblies. Journal of the American Chemical Society 2006;128:10988–9; (c) Zhang XJ, Tian YP, Jin F, Wu JY, Xie Y, Tao XT, et al. Self-assembly of an organic chromophore with Cd–S nanoclusters: supramolecular structures and enhanced emissions. Crystal Growth and Design 2005;5:565–70.

[7] Zhou HP, Li DM, Zhang JZ, Zhu YM, Wu JY, Hu ZJ, et al. Crystal structures, optical properties and theoretical calculation of novel two-photon polymerization initiators. Chemical Physics 2006;322:459–70.

[8] (a) Zhang SY, Chen XJ, Tian YP, Jin BK, Yang JX. Preparation and characterization of novel SeO_2/TiO_2 nanocomposite. Journal of Crystal Growth 2007; 304:42–6;
Zhang SY, Chen XJ, Tian YP, Jin BK, Yang JX. Preparation and characterization of novel SeO_2/TiO_2 nanocomposite. Journal of Crystal Growth 2007;304: 42–46. (b) Kong L, Li WJ, Li XL, Geng WQ, Hao FY, Wu JY, et al. Four divalent metal thiocyanate coordination compounds containing a rigid functional pyridine ligand. Polyhedron 2010;29:1575–82;
(c) Li L, Tian YP, Yang JX, Sun PP, Kong L, Wu JY, et al. Two-photon absorption enhancement induced by aggregation with accurate photophysical data: spontaneous accumulation of dye in silica nanoparticles. Chemical Communications 2010;46:1673–5.

[9] Hao FY, Zhang XJ, Tian YP, Zhou HP, Li L, Wu JY, et al. Design, crystal structures and enhanced frequency-upconverted lasing efficiencies of a new series of dyes from hybrid of inorganic polymers and organic chromophores. Journal of Material Chemistry 2009;19:9163–9.

[10](a) Fabbrini G, Menna E, Maggini M, Canazza A, Marcolongo G, Meneghetti M. Zinc-induced switching of the nonlinear optical properties of a functionalized bis(styryl)benzene. Journal of the American Chemical Society 2004; 126:6238–9;
(b) Kim HM, Jeong MY, Ahn HC, Jeon SJ, Cho BR. Two-photon sensor for metal ions derived from azacrown ether. Journal of Organic Chemistry 2004;69:5749–51.

[11](a) Tessore F, Roberto D, Ugo R, Pizzotti M, Quici S, Cavazzini M, et al. Terpyridine Zn(II), Ru(III), and Ir(III) complexes: the relevant role of the nature of the metal ion and of the ancillary ligands on the second-order nonlinear response of terpyridines carrying electron donor or electron acceptor groups. Inorganic Chemistry 2005;44:8967–78;
(b) Righetto S, Rondena S, Locatelli D, Roberto D, Tessore F, Ugo R, et al. An investigation on the two-photon absorption activity of various terpyridines and related homoleptic and heteroleptic cationic Zn(II) complexes. Journal of Material Chemistry 2006;16:1439–44.

[12](a) Heller M, Schubert US. Syntheses of Functionalized 2,2′:6′,2″-terpyridines. European Journal of Organic Chemistry 2003;6:947–61;
(b) Liu HQ, Cheung TC, Peng SM, Che CM. Novel luminescent cyclometaiated and terpyridine Gold(III) complexes and DNA binding studies. Journal of the Chemical Society, Chemical Communications 1995;17: 1787–8;
(c) Bonhôte P, Moser JE, Humphry-Baker R, Vlachopoulos N, Zakeeruddin SM, Walder L, et al. Long-lived photoinduced charge separation and redox-type photochromism on mesoporous oxide films sensitized by molecular dyads. Journal of the American Chemical Society 1999;121: 1324–36;
(d) Fang HJ, Du CM, Qu SL, Li YL, Song YL, Li HM, et al. Self-assembly of the [60]fullerene-substituted oligopyridines on Au nanoparticles and the optical nonlinearities of the nanoparticles. Chemical Physics Letters 2002; 364:290–6;
(e) Eryazici I, Moorefield CN, Durmus S, Newkome GR. Synthesis and single-crystal X-ray characterization of 4,4″-functionalized 4′-(4-bromophenyl)-2,2′:6′,2″-terpyridines. Journal of Organic Chemistry 2006;71:1009–14.

[13] Yang JX, Tao XT, Yuan CX, Yan YX, Wang L, Liu Z, et al. A facile Synthesis and properties of multicarbazole molecules containing multiple vinylene bridges. Journal of the American Chemical Society 2005;127:3278–9.

[14] Reynolds GA, Drexhage KH. New coumarin dyes with rigidized structure for flashlamp-pumped dye lasers. Optics Communication 1975;13:222–5.

[15] Hu ZJ, Yang JX, Tian YP, Tao XT, Tian L, Zhou HP, et al. Synthesis, structures, and optical properties of two novel two-photon initiators derived from 2,2′:6′,2″- terpyridine. Bulletin of the Chemical Society of Japan 2007;80: 986–93.

[16] Jin F, Li JF, Zhou HP, Wu JY, Yang JX, Tian YP, et al. Synthesis, crystal structures, and optical properties of a novel imidazole derivative and its Zn(II) complex. Journal of Molecular Structure 2007;829:202–7.

[17] Mongin O, Porres L, Kahn C, Pons T, Mertz J, Blanchard-Desce M. Synthesis and two-photon absorption of highly soluble three-branched fluorenylene-vinylene derivatives. Tetrahedron Letters 2003;44:8121–5.

[18](a) Zhou HP, Yin JH, Zheng LX, Wang P, Hao FY, Geng WQ, et al. Anion-induced assembly of different mercury coordination complexes and DFT calculations to evaluate weak interactions between similar double-helical chains. Crystal Growth and Design 2009;9:3789–98;
(b) Alvarez HM, Tran TB, Richter MA, Alyounes DM, Rabinovich D. Homoleptic group 12 metal bis(mercaptoimidazolyl)borate complexes M(BmR)2 (M = Zn, Cd, Hg). Inorganic Chemistry 2003;42:2149–56;
(c) Borovik AS, Bott SG, Barron AR. Arene–mercury complexes stabilized aluminum and gallium chloride: synthesis and structural characterization. Journal of the American Chemical Society 2001;123:11219–28.

[19] Lakowicz JR. Principles of fluorescence spectroscopy, vol. 298–300. New York: Kluwer Academic/Plenum; 1999. pp. 52–53, 648.

[20] Drobizhev M, Karotki A, Dzenis Y, Rebane A, Suo Z, Spangler CW. Strong cooperative enhancement of two-photon absorption in dendrimers. Journal of Physical Chemistry B 2003;107:7540–3.

[21] Jeong HC, Piao MJ, Lee SH, Jeong MY, Kang KM, Park G, et al. Octupolar dendrimers with large first hyperpolarizability. Advanced Functional Materials 2004;14:64–70.

[22] Xu C, Webb WW. Measurement of two-photon excitation cross sections of molecular fluorophores with data from 690 to 1050 nm. Journal of the Optical Society of America B 1997;13:481–91.

[23] Varnavski O, Goodson T, Sukhomlinova L, Twieg R. Ultrafast exciton dynamics in a branched molecule investigated by time-resolved fluorescence, transient absorption, and three-Pulse photon echo peak shift measurements. Journal of Physical Chemistry B 2004;108:10484–92.

[24] Albota MA, Xu C, Webb WW. Two-photon fluorescence excitation cross sections of biomolecular probes from 690 to 960 nm. Applied Optics 1998;37: 7352–6.